Int. J. Nano Dimens., 8 (4): 307-315, Autumn 2017

ORIGINAL ARTICLE

Sol-gel synthesis, characterization, optical properties and catalytic performance of $Y_2Ce_2O_7$ nanomaterial

Nadali Ramezani[1]; Morteza Enhessari[2]; Mohammad Yousefi[1]*

[1]*Department of Chemistry, Science and Research Branch, Islamic Azad University, Tehran, Iran*
[2]*Department of Chemistry, Naragh Branch, Islamic Azad University, Naragh, Iran*

Received 09 May 2017; revised 24 July 2017; accepted 23 August 2017; available online 28 August 2017

Abstract

$Y_2Ce_2O_7$ nano powders were synthesized via sol-gel reactions at 900 (S_1), 1000 (S_2) and 1100 (S_3) ˚C for 4 h using yttrium acetate ($C_6H_9O_6Y.xH_2O$), ammonium cerium nitrate ($(NH_4)_2Ce(NO_3)_6$) and stearic acid ($C_{18}H_{36}O_2$) as raw materials at stoichiometric 1:1 Y:Ce molar ratio. The synthesized materials were characterized by powder X-ray diffraction (PXRD) technique and Fourier transforms infrared (FTIR) spectroscopy. Structural analysis was performed by the *FullProf* program employing profile matching with constant scale factors. The results showed that the patterns had a main cubic $Y_2Ce_2O_7$ structure with space group of Fm3m. The data showed that the lattice parameters were increased with increasing the reaction temperature. FESEM images showed that the synthesized $Y_2Ce_2O_7$ particles had mono-shaped sphere morphologies. However, with increasing the reaction temperature to 1100 ˚C, the particle size scale was in micrometre range. Ultraviolet–visible spectra analysis showed that the nanostructured $Y_2Ce_2O_7$ powder (S_2) possessed strong light absorption property in the ultraviolet light region. The direct optical band gap was calculated as 3.15 eV. Besides, the photoluminescence spectrum for the obtained material (S_2) was investigated at λ_{ex}=230 nm as excitation wavelength. It showed a strong emission peak at 425 nm. Catalytic performance of the synthesized nanomaterial (S_2) was also investigated in alcohol oxidation reactions which showed excellent efficiency as 75%.

Keywords: *Nanocatalyst; Optical Properties; Oxidation; $Y_2Ce_2O_7$; Sol-gel.*

How to cite this article

Ramezani N, Enhessari M, Yousefi M. Sol-gel synthesis, characterization, optical properties and catalytic performance of $Y_2Ce_2O_7$ nanomaterial. Int. J. Nano Dimens., 2017; 8 (4): 307-315.

INTRODUCTION

Pyrochlore materials with general formula $A_2B_2O_7$ (where A is a medium-large cation and B is an octahedrally coordinated, high-charge cation) have been investigated for technological potential such as ferroelectric, magnetic, ionic conductors, catalysts, phosphors, radiation resistant materials properties [1-5]. Pyrochlore materials have attracted interests due to their ability to form substituted and defective structures, permitting interesting physical properties [6]. $Y_2Ce_2O_7$ is a mixed oxide composed of Y_2O_3 and CeO_2 ingredients. The material can exhibit the cooperative properties of the both mentioned oxides. Some of the properties of the oxides are mentioned bellow.

* Corresponding Author Email: *nadali.ramezani@srbiau.ac.ir*

CeO_2 is a functional material with a cubic fluorite structure. It is considered to be one of the important oxide materials because of its good thermal and chemical stability and special optical properties; for example, its high refractive index, optical transparency, high dielectric constant and non-toxicity. It can be used in several applications such as in optical coatings, electro-optical, microelectronic, and optoelectronic devices; as an ion-conducting layer electrolyte in solid oxide fuel cells; in oxygen gas sensors; as a support in automotive catalysts; and in ultraviolet shielding materials [7]. Also, Y_2O_3, has attracted attention due to several physical properties, such as high melting point, high mechanical strength, high thermal conductivity, large optical band gap, a

relatively high dielectric constant, a high refractive index, and very good protective behavior as a coating in severe reactive environments [8].

Different methods have been reported for the synthesis of $Y_2Ce_2O_7$ including sol-gel, hydrolyzed assisted precipitation, solid state, combustion, non-hydrolytic solution, spin pyrolysis and electrochemical precipitation methods [7].

In the present study, a sol-gel method was employed successfully to synthesize nanostructured $Y_2Ce_2O_7$ powders using yttrium acetate, ammonium cerium nitrate and stearic acid as raw materials at stoichiometric 1 : 1 Y : Ce molar ratio for the first time. To the best of our knowledge, there is no report on the synthesis of nanostructured $Y_2Ce_2O_7$ by the present method. UV-Vis and photoluminescence spectra of the obtained materials were also studied. Besides, catalytic performance of the obtained material was investigated for oxidation of alcohol.

EXPERIMENTAL

General remarks

All chemicals including yttrium acetate, ammonium cerium nitrate and stearic acid were of analytical grade, obtained from commercial sources (Sigma – Aldrich and Merck Company) and used without further purifications. Phase identifications were performed on a powder X-ray diffractometer SEIFERT XRD 3003 PTS using CuK_α radiation. The rietveld analyses were done by FullProf software with a χ^2 of 1.37 (S_1), 1.55 (S_2) and 1.37 (S_3) in profile matching mode. The morphology of the obtained materials was examined with a field emission scanning electron microscope (Hitachi FE-SEM model S-4160). Photoluminescence spectrum was recorded on a Perkin Elmer LF-5 spectrometer (PerkinElmer Inc., Waltham, MA, USA).

FTIR spectrum was recorded on a Tensor 27 (Bruker Corporation, Germany). Absorption spectrum was recorded on an Analytik Jena Specord 40 (Analytik Jena AG Analytical Instrumentation, Jena, Germany).

Preparation of cerium butoxide

In a typical experiment, 5.48 g (10 mmol) of $(NH_4)_2Ce(NO_3)_6$ was grinded in a mortar. The powder was then poured into a 250 mL beaker and then 60 mL of 1-buthanol was added to it drop-wise. This dissolution is a chemical reaction as demonstrated below:

$$4C_4H_9OH + (NH_4)_2Ce(NO_3)_6 \rightarrow$$
$$\rightarrow Ce(OC_4H_9)_4 + 2NH_4NO_3 + 4HNO_3$$

After the reaction was completed, cerium butoxide solution and a white precipitate were obtained. The cerium butoxide solution was separated by filtration [9, 10].

Cerium butoxide- stearic acid mixture

In a typical synthetic experiment, 11.38 g (40 mmol) of stearic acid was heated to 73 ˚C; then, the orange like obtained cerium butoxide solution from the previous section was added to the molten material. In this case a two-phase solution was achieved. The mixture was kept in an oven at 80 ˚C for 30 h. After the time, a homogeneous yellowish gel was cooled normally to the room temperature (product 1).

Preparation of yttrium acetate solution

2.67 g (10 mmol) of yttrium acetate ($C_6H_9O_6Y.xH_2O$) was powdered in a mortar and ground until a nearly homogeneous powder was obtained. The obtained powder was dissolved in a minimum HNO_3 65% (Product 2). Product 1 was poured into a beaker. It was molten on a heater and then product 2 was added to the liquid. The obtained material was kept in an oven and was heated at 80 ˚ C for 50 h. The beaker was heated on a heater and boiled at 180 to 200 ˚C. The temperature was increased to 350 ˚C and a black like viscose gel was obtained. The obtained gel was poured into a 25 mL crucible and heated in an electric oven at 900, 1000 and 1100 ˚C for 4 h. When the reaction was completed, the oven was cooled normally to the room temperature. The resultant powders were obtained.

RESULTS AND DISCUSSION

Characterization

The phase composition of the as prepared $Y_2Ce_2O_7$ nanomaterials was examined by powder X-ray diffraction technique. Fig. 1 (a, b and c) show the PXRD patterns of the obtained materials in the 2θ range 10-90°. The results of structural analyses performed by the *FullProf* program employing profile matching with constant scale factors are also included in the Fig. 1.

Red bars are the observed intensities while the black ones are the calculated data. The blue one is the difference: Yobs-Ycalc. The Bragg reflections positions are indicated by green bars. The patterns

have a well fitted defect pyrochlore structure profile with face centered cubic structure. The results showed that the patterns had main $Y_2Ce_2O_7$ structure. Lattice parameters were found as a=b=c= 5.38 to 5.40 Å and α=γ=β=90° with a space group of $Fm3m$ [11].

Table 1 shows the cell parameters data for $Y_2Ce_2O_7$ samples obtained by the rietveld analysis. It was found that the cell parameters were nearly constant with changing the reaction temperature. Also, the counts data, obtained from the vertical axes of the PXRD patterns shown in Fig. 1, showed that the count values were increased with increasing the reaction temperature. It indicates that the crystal growth was increased with increasing the reaction temperature. Besides, Table 1 shows the R_f, Bragg R_b factors and χ^2 to show the goodness of the fittings.

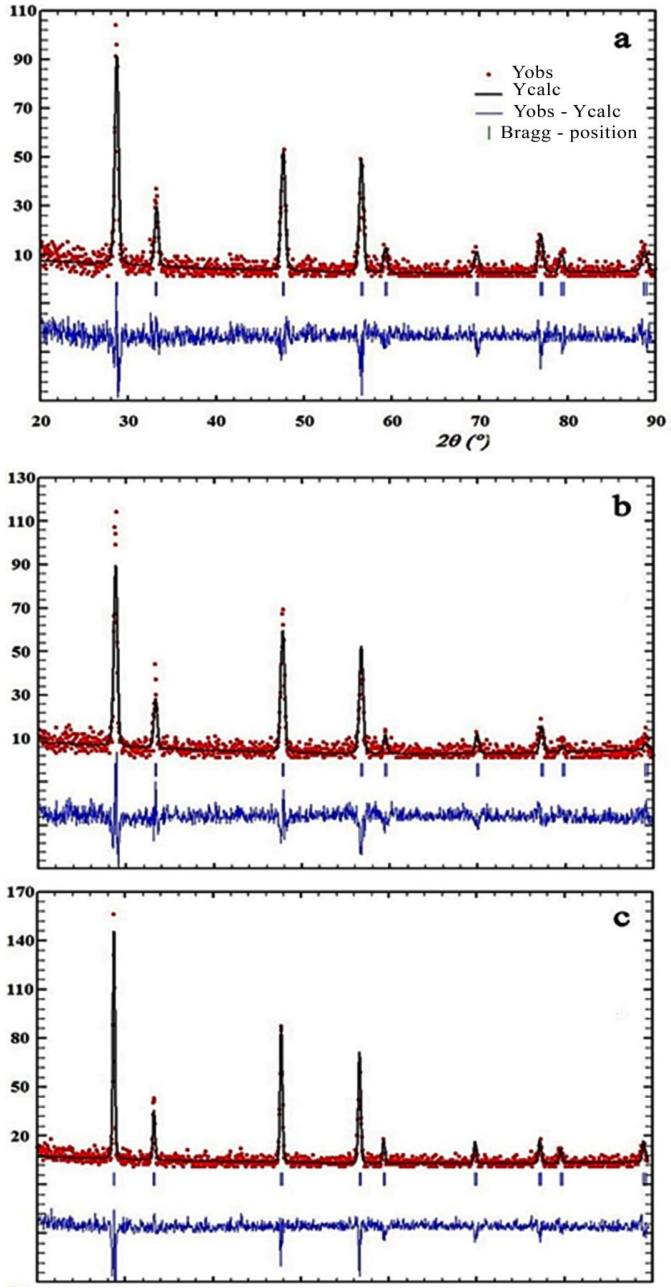

Fig. 1: PXRD patterns of the synthesized $Y_2Ce_2O_7$ nanomaterials and the rietveld analyses. Where (a) is S_1, (b) is S_2 and (c) is S_3.

Table 2 shows the crystal sizes of the as-synthesized nanomaterials in different reaction temperatures calculated from Scherrer equation, using the peak at h k l (111) corresponded to $Y_2Ce_2O_7$ phase;

$$t = \frac{k\lambda}{B_{\frac{1}{2}} \cos\theta}$$

In this equation, t is the entire thickness of the crystalline sample, λ is the x-ray diffraction wavelength (0.154 nm), and k is the Scherrer constant (0.9), $B_{1/2}$ of FWHM is the full width at half its maximum intensity and θ is the half diffraction angle at which the peak is located. The data mentioned in Table 2 show that the calculated crystal size for S_3 is larger than that of S_1. In other words, the crystal sizes become larger with increasing the reaction temperatures from 900 to 1100 ˚C that is in agreement with FESEM images.

Optical Properties

Fig. 2 shows the FTIR spectrum of the synthesized $Y_2Ce_2O_7$ (S_2). The spectrum shows that there are some peaks at around 440, 565, 897, 1204, 1637, 1720, 1930, 2853, 2918, 3441 and 3806 cm^{-1} that are the characteristic bands for $Y_2Ce_2O_7$. The band at 565 cm^{-1} is attributed to Y-O vibration [12]; however, the peaks of Y_2O_3 are in the ranges of 530-570 cm^{-1} and 660 – 700 cm^{-1} [13]; the bands at 440, 897 and 1204 cm^{-1} are attributed to the Ce-O vibration [14-17]. The peak at 1637 – 2000 cm^{-1} can be assigned to O-H bending vibration [18], the peaks at 1930 and 3441 cm^{-1} are attributed to O-H stretching vibration [19, 20].

UV–Vis absorption spectrum of the $Y_2Ce_2O_7$ nanomaterial (S_2) is shown in Fig. 3 a. The direct optical band gap is also shown in Fig. 3b. The pure $Y_2Ce_2O_7$ nanomaterial displayed typical visible absorption edge at about 420 nm. According to the results of Pascual *et al.* [21], the relation between the absorption coefficient and incident photon energy can be written as $(\alpha h\nu)^2 = A(h\nu - Eg)$, where A and Eg are constant and direct band gap energy, respectively.

The band gap energy was evaluated by extrapolating the linear part of the curve to the energy axis. It was found that the band gap was 3.15 eV. The value shows that the product can be used as efficient catalyst and photocatalyst.

Fig. 4 represents the room-temperature emission spectrum of the as-synthesized material (S_2) under excitation wavelength at 230 nm. The peak at 374 nm is due to the charge transfer from O^{2-} to Ce^{4+} [7]; the peak at about 400 – 425 nm is due to the charge transfer of O^{2-} to Y^{3+} [16]; the most intense peak at 425 nm is due to spin allowed transfer from the excited term ^3D to ^3P ($2_{[3/2]}0 \rightarrow 2_{[1/2]}0$) in Ce(IV) with the electronic configuration of $5p^5(^2P^0_{3/2})6s$ to $5p^5(^2P^0_{1/2})5d$ and Y(III) from $4p^54s$ to $4p^54d$ Martin et al.,1978 and Epstein et al.,1982 [22, 23].

Table 1: Cell parameter data calculated from rietveld analysis.

Sample	a (Å)	R_{Bragg}	R_F	χ^2	Counts
S_1	5.400484	2.42	2.63	1.37	104
S_2	5.381881	2.25	2.17	1.55	114
S_3	5.387026	2.54	2.11	1.37	158

Table 2: Scherrer data information for $Y_2Ce_2O_7$ nanomaterials.

	S_1	S_2	S_3
2θ	28.6057	28.7067	28.6787
FWHM	0.53509	0.51534	0.28624
$B_{1/2}$	0.009334	0.008990	0.004993
cos (θ)	0.9690	0.9688	0.9688
t (nm)	15	16	29
d (Å)	3.117	3.106	3.109

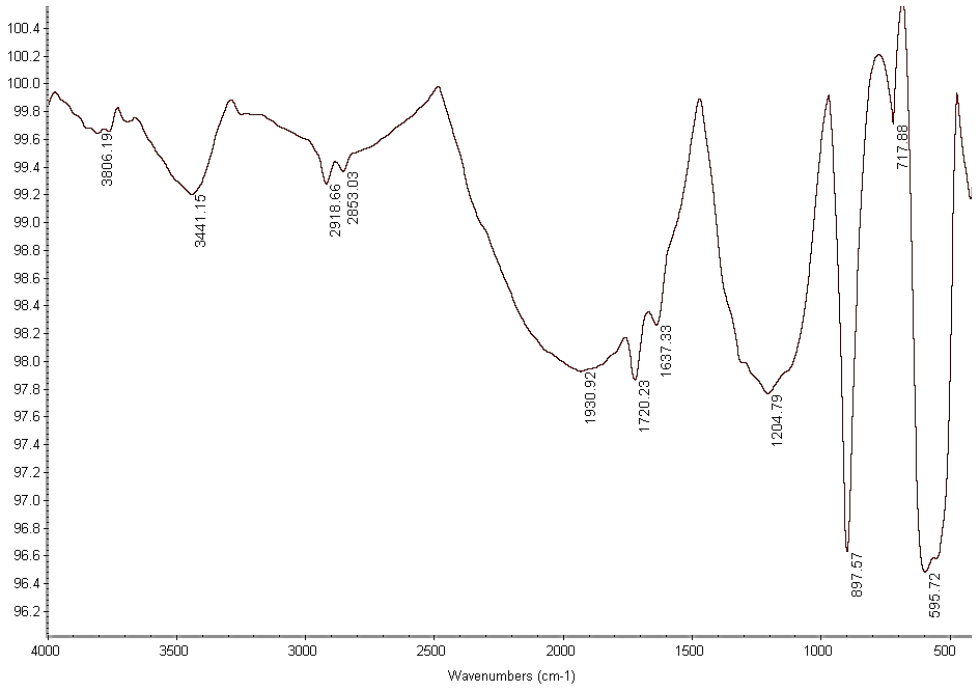

Fig. 2: FTIR spectrum of S_2.

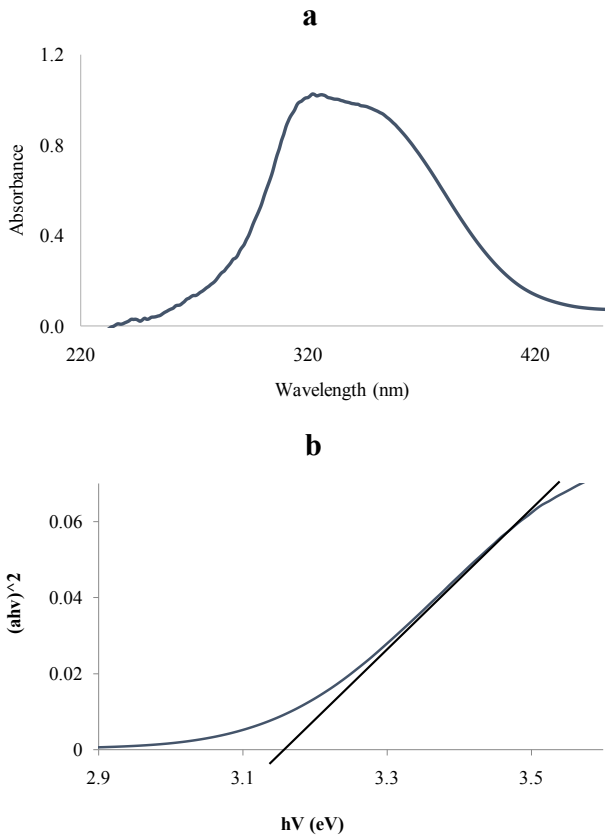

Fig. 3: Plots of a) UV-Vis spectrum and b) $(\alpha h\nu)^2$ versus $h\nu$ for $Y_2Ce_2O_7$.

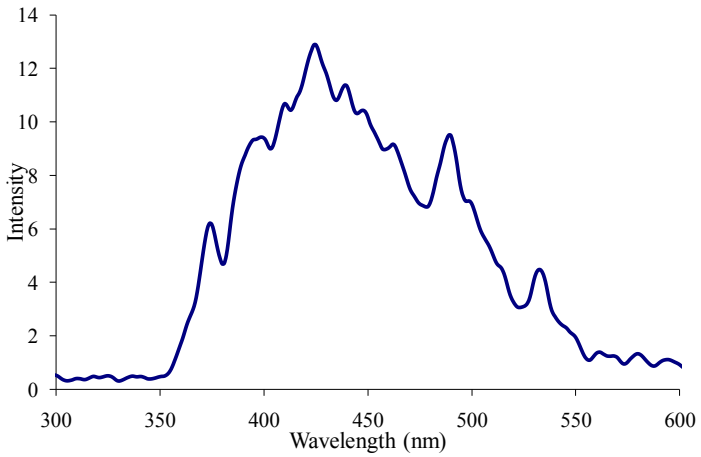

Fig. 4: The photoluminescence spectrum of S_2 at λ_{ex} = 200 nm.

Paint parameters

Table 3 represents the data obtained from paint physics laboratory. The c* parameter value indicates the high purity of the product. According to the L* value, the white color of the material is confirmed. The H* value is 93.1 that is corresponded to the lime and emerald color region. The data are in good agreement with reference [24].

Fig. 5 shows the maximum reflectance of the as synthesized material (S_2). It shows the value of about 75%. The reflectance amount occurs in the infrared region. So the pigment is classified in the cold color region and can be used as an insulator coat against heat.

Morphology

Fig. 6 (a-c) shows the FESEM images of the as synthesized $Y_2Ce_2O_7$ at 900 (S_1), 1000 (S_2) and 1100 (S_3) ˚C. It is apparent from Fig. 6a that the particle sizes are about 20- 40 nm. Fig. 6b shows that the particle sizes are about 30-60 nm. However, it was found from Fig. 6c that when increasing the reaction time to 1100 ˚C, the particle size scale was in micrometer range. It shows that sufficient temperature for the synthesis of $Y_2Ce_2O_7$ nano powder is up to 1000 ˚C. So, the data shows that the particle sizes become larger with increasing the reaction temperature. The conclusion is in agreement with the calculated data from Scherrer equation.

Catalytic application

The catalytic activity of S_2 was investigated for the oxidation of benzyl alcohol derivative compounds. H_2O_2 and TBHP *(Tert-Butyl Hydroperoxide)* were used as the oxidants. The data for the catalytic performance using S_2 are included in Table 4. High yield for the process was obtained when the solvent was acetonitrile. According to the Fig. 7, benzyl alcohol was used as precursor. Different products were obtained with changing the amine derivative type compounds. Catalytic oxidation reactions have been done in present of $Y_2Ce_2O_7$ nanopowders as catalyst and benzyl alcohol as a precursor with an efficiency of 75 %. Due to the types of second stage amines, secondary amines products with cyanide functional group are accessible. High efficiency, using water as a green solvent and using hydrogen peroxide as an oxidizing agent with water as byproduct, make this method an environmental friend and a clean design of chemical process.

A simple and convenient method is reported for the effective conversion of benzyl alcohol and its derivatives to their corresponding aldehydes in the presence of nano structured ZnO as the catalyst. According to the results, this method has high reaction rates, high yields of the products, and the best advantage of this oxidation is solvent-free condition [25].

Ozonation of benzyl alcohol and benzaldehyde in acetic acid was studied. Use of Co(II) acetate as a catalyst makes it possible to raise the consumption rates of benzyl alcohol and benzaldehyde. The yield of benzoic acid increases to 95.4% in oxidation of the alcohol and to 91.2% in oxidation of the aldehydes [26].

The photocatalytic oxidation of benzyl alcohol and its derivatives into corresponding aldehydes proceeded at high conversion and selectivity on

Table 3: Color characteristic data of S_2.

Color parameter	L^*	a^*	b^*	c^*	H^*
Data	85.57	-0.61	11.16	11.18	93.10

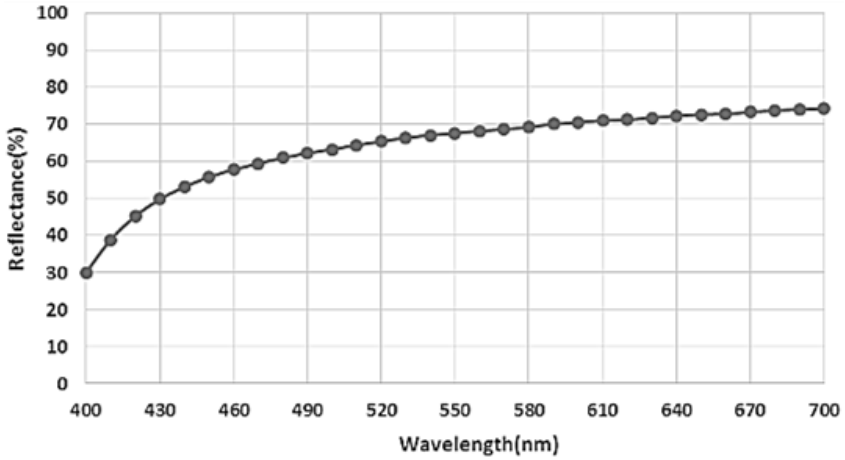

Fig. 5: Color characteristic test graph.

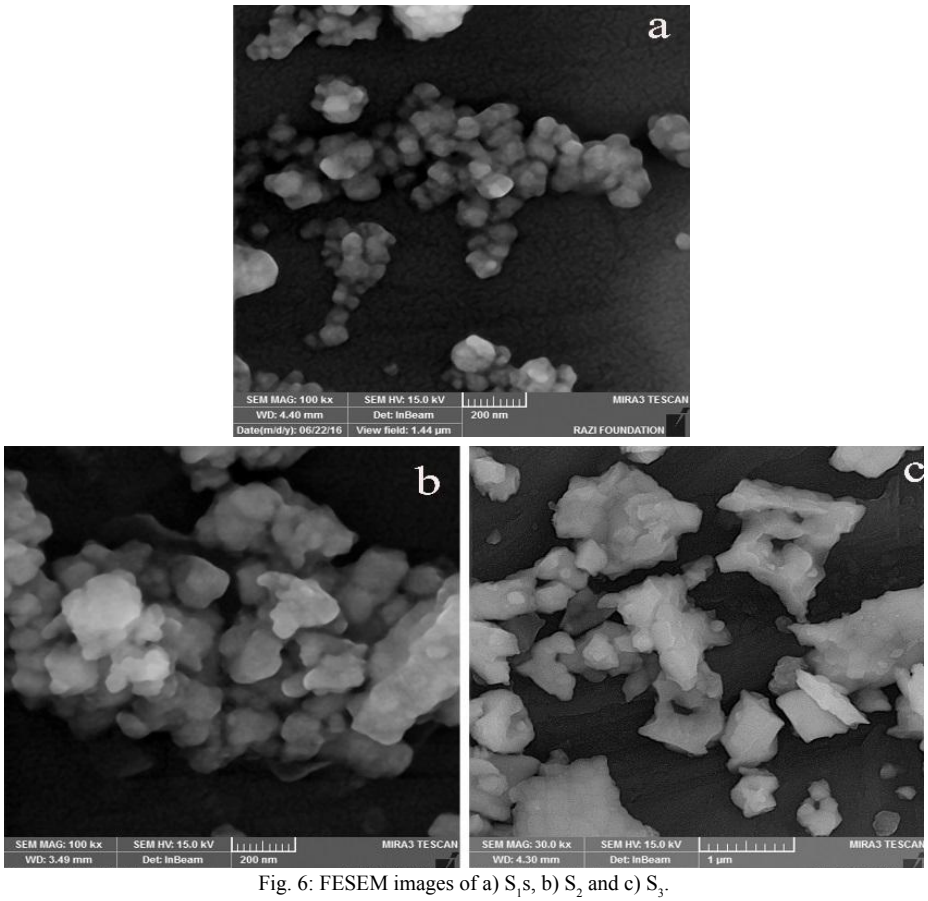

Fig. 6: FESEM images of a) S_1s, b) S_2 and c) S_3.

Table 4: Catalytic performance data. Condition: Benzyl alcohol (1 mmol), Oxidant (1 equivalent), Aniline (1 equivalent), tetrametyl silyl cyanide (1.2 equivalent), solvent (3 mL) under argon atmosphere.

Entry	$Y_2Ce_2O_7$(mg)	Oxidizing	Solvent	Temperature(°C)	Yeild %
1	10	TBHP	Water	60	30
2	10	TBHP	Methanol	60	20
3	10	TBHP	Ethanol	60	30
4	10	TBHP	Acetonitrile	60	55
5	10	H_2O_2	Acetonitrile	60	70
6	20	TBHP	Acetonitrile	60	75
7	40	TBHP	Acetonitrile	60	75
8	10	TBHP	Acetonitrile	R.T*	45
9	10	TBHP	Acetonitrile	40	50
10	-	TBHP	Acetonitrile	60	10
11	10	-	Acetonitrile	60	-

*R.T=Room Temperature

a Tio_2 photocatalyst under o_2 atmospher. Here the propertices of the surface complex as the active center for this selective photocatalytic oxidation and the mechanism behind the reaction have been investigated [27].

Selective Aerobic Oxidation of Benzyl Alcohol Driven by Visible Light on Gold Nanoparticles Supported on Hydrotalcite Modified by Nickel Ion. A series of hydrotalcite (HT) and hydrotalcite modified by the transition metal ion Ni(II) was prepared with a modified coprecipitation method before being loaded with gold nanoparticles. The gold supported on Ni3Al hydrotalcite with a Ni^{2+}/Al^{3+} molar ratio of 3:1 was investigated. A single-phase catalyst with high crystallinity, a layered structure and good composition was successfully fabricated. Good conversions and superior selectivities in the oxidation of benzyl alcohol and its derivatives were obtained with visible light due to the effect of localized surface plasmon resonance (LSPR) of gold nanoparticles and the synergy of the transition metal ion Ni(II). This reaction was proven to be photocatalytic by varying the intensity and wavelength of the visible light. The catalyst can be recycled three times. A corresponding photocatalytic mechanism of the oxidation reaction of benzyl alcohol was proposed [28].

The reactions were carried out in a 50 mL round-bottom flask with a magnetic stirrer. In a typical run, a mixture of benzyl alcohol (1 mmol), oxidant (1 equivalent), Aniline (1 equivalent), tetrametyl silyl cyanide (1.2 equivalent) and solvent (3 mL) was transferred into the reactor under argon atmosphere. Then, the solution was intensively stirred at 60°C and 1 atm. The reactions were followed by gas chromatography (GC) and the structures of the products were confirmed by GC-MS (Finnigan Company, Silicon valley, CA, USA). The catalyst and reactants were separated via centrifugation. It seams that surface complex formed by the adsorption of a benzyl alcohol compound. This absorption is due to the surface complex between $Y_2Ce_2O_7$ nanopowders and benzyl alcohol. It is assigned to the charge transfer from benzyl alcohol to $Y_2Ce_2O_7$ nano powder on the surface complex.

CONCLUSION

$Y_2Ce_2O_7$ nano-powders were prepared by sol-gel method at different reaction temperatures. It was found that the product was crystallized in the cubic crystal structure. The reaction temperature was found to have main effect on the crystal growth and particle size. The direct band gap was calculated as 3.15 eV. The photoluminescence property was studied at λ_{ex}=230 nm. It was found that the material had a maximum emission at 425 nm that is in the visible light region. The catalytic performance of the obtained material was studied for the oxidation of alcohol. The yield was found 75%. From the catalytic process, several amine and derivative ones products can be obtained.

CONFLICT OF INTEREST

The authors declare that there is no conflict of interests regarding the publication of this manuscript.

REFERENCES

[1] Sharma N., Subba Rao G. V., Chowdhuri B. V. R., (2006), Anodic properties of tin oxides with pyrochlore structure for lithium ion batteries. *J. Power Sources.* 159: 340-344.

[2] Mandal B. P., Garg N., Sharma S. M., Tyagi A. K., (2006), Preparation, XRD and Raman spectroscopic studies on new compounds $RE_2Hf_2O_7$ (RE= Dy, Ho, Er, Tm, Lu, Y): Pyrochlores or defect-fluorite?. *J. Solid State Chem.* 179: 1990–1994.

[3] Li T., Zhang K., Wang H., Yan H., (2006), Low-temperature synthesis and structure characterization of the serials $Y_{2-\delta}Bi_\delta Sn_2O_7$ ($\delta = 0-2.0$) nanocrystals. *J. Solid State Chem.* 179: 1029–1034.

[4] Zhu H. L., Yang D. R., Zhu L. M., Li D. S., Chen P. H., Yu G. X., (2007), Hydrothermal synthesis and photoluminescence properties of $La_{2-x}Eu_xSn_2O_7$ (*x*=0–2.0) nanocrystals. *J. Am. Ceram. Soc.* 90: 3095–3098.

[5] Sickafus K. E., Minervini L., Grimes R. W., Valdez J. A., Ishimaru M., Li F., McClellan K. J., Hartmann T., (2000), Radiation tolerance of complex oxides. *Science.* 289: 748–751.

[6] Sellami M., Caignaert V., Hamdad M., Belarbi A., Sari-Mohamed I., Bahmani A., Bettahar N., (2011), Synthesis and characterization of the new pyrochlore $Bi_{1.5}Sb_{1.5-x}Nb_xMnO_7$. *Solid Solution. C. R. Chimie.* 14: 887-890.

[7] Raj A. K. V., Prabhakar R. P., Sreena T. S., Sameera S., James V., Renju U. A., (2014), Remarkable changes in the photo luminescent properties of $Y_2Ce_2O_7$: Eu^{3+} red phosphors through modification of the cerium oxidation states and oxygen vacancy ordering. *Phys. Chem. Chem. phys.* 2014: 23699-23706.

[8] Momeni Larimi Z., Amir abadizadeh A., Zelati A., (2011), Synthesis of Y_2O_3 nanoparticles by modified transient morphology method. *Int. Conf. Chem. Chem. Proc.*

[9] Enhessari M., Ozaee K., Shaterian M., Karamali E., (2013), Strontium cerate nanoparticle synthesis method. Pub. No.: US8512654 B_2.

[10] Enhessari M., (2013), Synthesis, characterisation and optical band gap of $Cr_{1.3}Fe_{0.7}O_3$ nanopigments. *Pigm. Resin. Technol.* 42: 347-352.

[11] Honghui J., Weixiong Y., Xiaolin L., Jinsheng L., Ping W., Bin Y., (2013), Yb^{+3} and Er^{+3} co-doped $Y_2Ce_2O_7$ nanoparticles: Synthesis and spectroscopic properties. *Bullet. Mater. Sci.* 36: 1147-1151.

[12] Miller F. A.,Wilkins C. H., (1952), Infrared spectra and characteristic frequencies of inorganic ions. *Anal.Chem.* 24: 1253-1294.

[13] Sheibley D. W., Fowler M. H., (1966), Infrared spectra of various metal oxides in theregion of 2 to 26 microns. nasatn d-3750. Lewis Research Center: Cleveland, Ohio. Accessed August 7, 2015.

[14] DeKock R. L., Weltner Jr. W., (1971), Spectroscopy of rare earth oxide molecules in inert matrices at 4.deg.K. *Phys. Chem.* 75: 514-519.

[15] Gabelnick S. D., Reedy G. T., Chasanov M. G., (1974), Infrared spectra and structure of some matrix isolated lanthanide and actinide oxides. *Chem. Phys.* 60: 1167-1172.

[16] Palard M., Balencie J., Maguer A., Hochepied J., (2010), Effect of hydrothermal ripening on the photoluminescence properties of pure and doped cerium oxide nanoparticles. *Mater. Chem. Phys.* 120: 79-88.

[17] NIST Standard Reference Database Number 69., (2016). NIST Chemistry Web Book. *National Institute of Standards and Technology.* United States of America.

[18] Vahur S., Teearu T., Peets P., Joosu L., Ivo Leito L., (2016), ATR-FT-IR spectral collection of conservation materials in the extended region of 80-4000 cm^{-1}. *Anal. Bioanal. Chem.* 408: 3373-3379.

[19] Nakamoto, K., (2009), Infrared and raman spectra of inorganic and coordination compounds, Part A, Theory and Applications in Inorganic Chemistry, 6th Edition. *John Wiley & Sons*, Inc.

[20] Russell S., (1977), Physical methods in inorganic chemistry. Urbarm Reillhold Publishil, g Coq., New York.

[21] Pascual J, Camassel J., Mathieu M., (1978), Fine structure in the intrinsic absorption edge of TiO_2. *Phys. Rev. B: Solid State.* 18: 5606-5614.

[22] Martin W. C., Zalubas R., Hagan L., (1978), Atomic energy levels-the rare-earth elements, The Spectra of Lanthanum, Cerium, IBSNBS, Washington, D.C 20234.

[23] Epstein G. L., Reader J., (1982), Spectrum and energy levels of triply ionized Yttrium. *J. Opt. Am.* 72: 476-492.

[24] Zhao M., Han A., Ye M., Wu T., (2013), Preparation and characterization of Fe^{3+} doped $Y_2Ce_2O_7$ pigments with high near-infrared reflectance. *Solar Energy.* 97: 350–355.

[25] Sadeghi S., MalekiIranian F., (2011), Solvent free oxidation of benzyl alcohol and its derivatives into corresponding aldehydes on nano structured ZnO as catalyst. *J. Organic Chem.* 3: 635-637.

[26] Potapenko E. V., Andreev P. Yu., (2010), Oxidation of benzyl alcohol and benzaldehyde with ozone in acetic acid. *Russian J. Applied Chem.* 83: 1243−1247.

[27] Higashimoto S., Kitao N., Yoshida N., Sakura T., Azuma m., Ohue H., Sakata Y., (2009), Selective photocatalytic oxidation of benzyl alcohol and its derivatives into corresponding aldehydes by molecular oxygen on titanium dioxide under visible light irradiation. *J. Catalysis.* 266: 279-285.

[28] Guo D., Wang Y., Zhao P., Bai M., Xin H., Guo Z., Li J., (2016), Selective aerobic oxidation of benzyl alcohol driven by visible light on gold nanoparticles supported on hydrotalcite modified by nickel Ion. *Catalysts.* 6: 64-69.